Research Square

Preprints are preliminary reports that have not undergone peer review.
They should not be considered conclusive, used to inform clinical practice,
or referenced by the media as validated information.

Maternal diet-induced excess adiposity programs multisystem vulnerability that is unmasked by postnatal infection challenge

Tatiane Ribeiro
McMaster University
Anastasia Warmington
McMaster University
Erica Yeo
McMaster University
Christian Bellissimo
McMaster University
Brianna Kennelly
McMaster University
Braeden Cowbrough
McMaster University
Patrycja Jazwiec
McMaster University
Jessica Breznik
University of Guelph
Erica DeJong
McMaster University
Katherine Kennedy
McMaster University
Janine Strehmel
McMaster University
Madison McKellar
McMaster University
Ariana Lewis
McMaster University
Dawn Bowdish
McMaster University
Deborah Sloboda
sloboda@mcmaster.ca

McMaster University

Article

Keywords: Maternal excess adiposity, pneumonia, infection challenge, intestinal function, immunophenotype

Posted Date: July 8th, 2026

DOI: https://doi.org/10.21203/rs.3.rs-9733486/v1

License: This work is licensed under a Creative Commons Attribution 4.0 International License. Read Full License

Additional Declarations: No competing interests reported.

Version of Record: A version of this preprint was published at Scientific Reports on September 18th, 2026. See the published version at https://doi.org/10.1038/s41598-026-71711-y.

Abstract

Excess adiposity before and during pregnancy has been linked to cardiometabolic inflammatory disease in offspring, yet programmed vulnerabilities may remain latent until challenge. Using a mouse model of maternal high-fat diet (mHF)-induced excess adiposity, we investigated whether maternal excess adiposity programs immune, intestinal, and metabolic vulnerabilities that emerge after postnatal Streptococcus pneumoniae challenge. Wildtype C57BL/6J female mice were fed either standard chow or a high-fat diet before conception and throughout pregnancy and lactation. Offspring were assessed during neonatal life and again in adulthood before and after intranasal Streptococcus pneumoniae challenge. Neonates born to high-fat-diet-fed mothers showed elevated expression of inflammatory mediators (Ptafr, Tlr2, Tlr4) and decreased surfactant proteins (Sftpa, Sftpb, Sftpc) in the lung, indicating dysregulated host defence at birth. Before infection, adult mHF offspring had reduced circulating leukocytes and altered glucose handling. Although mHF did not alter acute pneumococcal burden, recovery was associated with increased intestinal permeability, altered intestinal morphology, shifts in cecal microbial community structure, and changes in glucose-insulin homeostasis. Several outcomes were sex dependent, indicating that maternal excess adiposity programs organ-specific and sex-specific responses to postnatal challenge. These findings suggest that maternal adiposity establishes vulnerabilities in immune, intestinal, and metabolic systems that become evident after inflammatory stress.

Introduction

The prevalence of obesity, characterized by excess adiposity and often dysregulated metabolic function, continues to rise among individuals of reproductive age posing significant challenges for maternal and offspring health.[1–3] Numerous experimental and epidemiological studies have shown that maternal excess adiposity is associated with maternal insulin resistance, dysregulated immune signaling, and altered nutrient transport at the maternal–fetal interface.[4,5] These changes can induce sex-specific modifications in fetal development, with lasting effects on offspring health, and susceptibility to chronic conditions such as hypertension and hyperlipidemia.[3,6] While considerable attention has focused on cardiometabolic outcomes, [7] less is understood about the pathways by which maternal excess adiposity shape offspring immune function and susceptibility to repiratory infection. [8]

Adverse exposures during critical developmental windows have been shown to contribute to increased risk of lung disease, including both respiratory and chronic inflammatory airway conditions.[9] Maternal excess adiposity is associated with impairments in lung structure and function that predispose offspring to asthma and other chronic airway diseases and an increased childhood risk of respiratory infections and infection-related hospitalizations.[10–13] Thus, even after recovery, early-life respiratory infections may precipitate prolonged dysregulation of immune homeostasis within the lung, contributing to increased susceptibility to chronic lung conditions.[14]

Respiratory inflammatory responses (including allergy and asthma) in offspring are thought to be driven in part, by chronic low-grade intrauterine inflammation and altered cytokine signaling during gestation.[15–20] Expanding maternal adipose depots likely contribute to this pro-inflammatory uterine milieu,[21,22] although emerging evidence has also implicated impaired maternal gut barrier function and shifts in the maternal and offspring gut microbiome as other potential mediators of offspring immune dysregulation. [23]

We have previously shown that diet-induced excess adiposity before and during pregnancy impairs maternal intestinal barrier function, alters immune cell populations in distal portions of the maternal intestine, and results in an altered maternal immunophenotype. [24,25] These changes in maternal gut barrier function likely contribute to a proinflammatory intrauterine environment which in turn can impair fetal gut development and alter the course of early intestinal colonization.[26] Consequently, these developmental changes combined with disrupted postbirth microbial colonization during the critical first 1000 days, alter the trajectory of healthy metabolic and immune maturation.[27–29,30,31] Such disruption to early life colonization and increased permeability can potentiate postnatal lung inflammation through the translocation of microbial products and metabolites as well as systemic cytokine release, contributing to respiratory inflammatory responses in offspring. [32,33]

Indeed, emerging data suggest that maternal inflammatory states can disrupt offspring gut barrier integrity and immune function in organs distal to the gut, including the lung,[34–38] leading to intestinal dysbiosis that is associated with altered respiratory microbial composition and consequent changes in pulmonary immune responses.[12,39,40] Increased maternal cytokine production in the context of obese pregnancies has been shown to impair fetal lung development.[41] Thus, disrupted intestinal barrier function and microbiome–immune crosstalk during critical developmental windows may underlie both immune and metabolic vulnerability in offspring.

While adverse developmental exposures can induce lasting physiological changes, their functional relevance often only becomes apparent following a postnatal challenge. Previous work shows that a secondary postnatal insult, such as infection or dietary stress, often reveals underlying programmed vulnerabilities, including those found in the immune system.[42–44] Therefore, in the current study we investigated whether prenatal exposure to maternal excess adiposity and a postnatal infection challenge interact to influence offspring immunophenotype, and metabolic and gut function. Here, we used postnatal *Streptococcus pneumoniae* respiratory challenge as an inflammatory stressor to test whether maternal high-fat diet-induced excess adiposity in mice[4,24,25,45] programs latent deficits in offspring immune–metabolic resilience. We therefore evaluated neonatal lung immune markers and adult circulating immune profiles, insteantial barrier function and morphogoly, cecal intestinal microbial profiles, and systemic glucose homeostasis at before and after infection challenge.

Methods

Animal model of maternal excess adiposity

All animal procedures were approved by the institutional ethics board and performed following CCAC guidelines (AUP AUP-24-27, 21-04-13). Six-week-old C57BL/6J male and female mice (Jackson Laboratory, Cat. No. 000664) were housed under specific pathogen-free conditions at the McMaster University Central Animal Facility in vent-rack cages at 22°C on a 12-hour light/dark cycle. To generate primiparous females, female and male mice were time-mated to generate a first pregnancy, and all neonatal offspring (weighing approximately 2.5–3g) were euthanized by decapitation at postnatal day 3 (P3). After one week of recovery from the first pregnancy, primiparous female mice were randomized to receive either a control chow diet (CTL, 17% kcal fat, 54% kcal carbohydrates, 29% kcal protein, 3 kcal/g; Harlan 8640 Teklad 22/5 Rodent Diet) or a high-fat diet (mHF, 45% kcal fat, 35% kcal carbohydrates, 20% kcal protein, 5.21 kcal/g, Research Diets Inc. D12451) *ad libitum* for two weeks, followed by overnight timed mating. Successful mating was identified the next morning by the presence of a vaginal plug (designated embryonic day E0.5 of pregnancy). Pregnant dams were singly housed and remained on CTL or mHF diets throughout pregnancy and lactation.

Following delivery, all second litters were standardized to six pups per dam, with equal numbers of each sex where possible to ensure standard pup nutrient intake across groups. Serum and lung tissue samples were collected from a subset of pups (weighing approximately 5–6g) were euthanized by decapitation at P7; body weight and adiposity were assessed using the Lee Index (an anthropometric proxy for adiposity/obesity in rodents, conceptually analogous to BMI in humans; [body weight (g)]^1/3 / [naso–anal length (cm)] × 1000).[46] On postnatal day 21 (P21), offspring were weaned, housed by sex (3 mice per cage), and received a healthy aging diet *ad libitum* (kcal: 13% fat, 67% carbohydrates, 20% protein, Teklad irradiated global rodent Diet 2914). Offspring body weights were recorded weekly until postnatal day 60 (P60), and monthly from P60 until postnatal day 120 (P120). Our experimental design is illustrated in Fig. 1. Subsets of offspring from CTL and mHF dams underwent glucose tolerance testing, gut barrier function, and immunophenotyping prior to tissue collection two weeks before (P90) and then after (P120) the infection challenge.

Postnatal infection challenge

To investigate whether early life exposure to maternal excess adiposity interacts with postnatal stressors, offspring were challenged with a respiratory bacterial infection. Male and female offspring (weighing approximately 18–25g) were anesthetized with isoflurane and intranasally inoculated with $1x10^4$ colony-forming units (CFUs) of *Streptococcus pneumoniae* (P1542 serotype 4, in 40 µL PBS) at P90,[47] and were monitored twice a day for body weight and clinical condition, including activity, posture, and coat appearance. Body weight loss of ~ 5% was used as an early indicator of disease progression. Humane endpoints were defined as ≥ 10% body weight loss or the presence of severe clinical signs of distress, including piloerection, hunched posture, periocular closure, moribund state, respiratory distress, reduced spontaneous movement, lethargy, social isolation, and abnormal hyperactivity at which point

animals (weighing approximately 14–20g) were anesthetized with isoflurane and euthanized by cervical dislocation in accordance with institutional guidelines.[47] During the infection period, offspring were regularly monitored and provided with hydration gel (Hydrogel ClearH2O, 70-01-5022) and a protein/carbohydrate supplement (Ensure® regular, Saint-Laurent, QC) *ad libitum*to ensure proper hydration and nutrition. To investigate potential differences in peak bacterial load, a subset of infected mice (weighing approximately 18–25g) were anesthetized with isoflurane and euthanized by cervical dislocation three days post-inoculation (acute infection, P93) (n = 6/group/sex) and central nasal turbinate (CNT) *S. pneumoniae* CFUs were counted as per published protocols.[47,48]

Pre- and post-infection in vivo measures of glucose metabolism and gut function in offspring:

Oral glucose tolerance test (OGTT)

Oral glucose tolerance was assessed in offspring two weeks before (P90, pre-infection) and ~ 30 days after (P120, post-infection) infection by oral gavage with D-glucose (G5767; Sigma-Aldrich; 2g/kg). Prior to the test, offspring were fasted for 6 hours, after which offspring blood glucose levels were measured through tail vein sampling using a MediSure Blood Glucose Meter (MEDIS-DG001MM), 30 minutes before (-30), immediately prior to (0), and 15, 20, 30, 40, 60, 90, and 120 minutes after glucose administration.

In vivo intestinal permeability

Intestinal permeability was evaluated at two weeks before (P90 pre-infection) and ~ 30 days after (P120, post-infection) by measuring plasma fluorescence levels after oral gavage of 500mg/kg body weight 4-kDa FITC-dextran (Sigma-Aldrich, #46944) diluted in PBS (pH 7.4; 1.8 mM KH_2PO_4, 2.7 mM KCl, 10 mM Na_2HPO_4, 137 mM NaCl). All mice fasted for 12 hours overnight before gavage. Blood was collected via tail vein immediately prior to (0) and 30, 60, 90, 120, and 240 minutes after gavage. Blood was centrifuged at 5,000 rpm for 10 minutes to collect plasma. Plasma was diluted 1:10 in PBS in flat-bottom 96-well black plates, and fluorescence was measured using a spectrophotometer (excitation: 485 nm, emission: 530 nm; Synergy H4 Hybrid Microplate Reader, BioTek Instruments, Inc.). For each mouse, plasma fluorescence was calculated by subtracting the baseline fluorescence measurement, as we have previously published.[25]

Tissue and cecal sample collections

Subsets of offspring of each sex (weighing approximately 20–26g) were anesthetized with isoflurane and euthanized by cervical dislocation at both pre-infection (P90) and post-infection (P120) timepoints. At these times, whole blood was collected retro-orbitally and processed for measures of serum insulin

and for immunophenotyping by flow cytometry (see below). Offspring organs weights (liver, heart, lung, spleen, thymus, cecum) and intestinal length were recorded. Cecal contents were collected for microbial sequencing (see below) and intestinal gut sections (small intestine, colon) were collected for intestinal morphology (see below).

Insulin ELISA

Serum insulin concentrations were quantified using a commercially available insulin immunoassay kit (32380; Toronto Bioscience) as per the manufacturer's instructions using a Synergy H4 Hybrid microplate reader (BioTek Instruments). Insulin concentrations were interpolated from a four-point standard curve.

Offspring Immunophenotyping

The numbers and frequencies of circulating leukocyte populations, including B cells, $CD4^+$ and $CD8^+$ T cells, NK cells, neutrophils, and monocytes, were determined at pre-infection (P90) and ~ 30 days following infection (P120) in offspring using flow cytometry Whole blood was collected by retro-orbital bleed under isoflurane anesthesia using a heparinized hematocrit tube and stored in a microfuge tube with 10 µl heparin. 100 µl of whole blood per immunophenotyping panel was stained for 30 minutes at room temperature in the dark with monoclonal fluorochrome-conjugated antibodies (Supplementary Table 1) diluted in FACS buffer (0.5% w/v BSA, 5mM EDTA in phosphate-buffered saline, pH 7.4), with inclusion of isotype and unstained controls. Stained samples were treated with 1-step Fix/Lyse Solution (eBioscience™, Cat. No. 00-5333-54; diluted 1:10 in dH_2O) for 10 minutes to deplete erythrocytes and preserve surface staining, washed once in FACS buffer, and resuspended in 245 µl of FACS buffer. Absolute cell counts were determined using CountBright absolute cell counting beads (5 µl/sample, Life Technologies, Ontario, Canada Cat. No. C40000). Samples were acquired using an LSR Fortessa flow cytometer (BD Biosciences). Data were analyzed using FlowJo version 10.10 software (BD Biosciences).

Microbial sequencing: 16s rRNA gene sequencing and analysis

Cecal samples were collected from mice at P90 and P120 for 16s rRNA gene sequencing as previously described.[49,50] Genomic DNA was extracted following Stearns *et al.* with modifications. [51] Briefly, samples were transferred to screw-cap tubes containing 2.8 mm ceramic beads, 0.1 mm glass beads, Guanidinium–EDTA–Sarkosyl buffer (GES), and sodium phosphate buffer. After bead-beating and centrifugation, the supernatant was processed using the KingFisher Apex 96-Deep Well Magnetic Particle Processor (Thermo Scientific) with the Multi-Sample Kit (Life Technologies #4413022).

The V3–V4 region of the 16S rRNA gene was amplified using primers 341F (CCTACGGGNGGCWGCAG) and 806R (GGACTACNVGGGTWTCTAAT) with Illumina adapters, as described in Bartram *et al.* (doi:

10.1128/AEM.02772-10). PCR was performed with 50 ng DNA, 1 U Taq, 1× buffer, 1.5 mM $MgCl_2$, 0.4 mg/mL BSA, 0.2 mM dNTPs, and 5 pmol of each primer. Cycling conditions were: 94°C for 5 min; 5 cycles of 94°C for 30 s, 47°C for 30 s, 72°C for 40 s; 25 cycles of 94°C for 30 s, 50°C for 30 s, 72°C for 40 s; and a final extension at 72°C for 10 min. Amplicons were visualized on a 1.5% agarose gel, normalized by band intensity, and pooled for sequencing on the Illumina MiSeq platform (2×300 bp, McMaster Genomics Facility).

Adapter and primer sequences were removed using Cutadapt (doi: 10.14806/ej.17.1.200), with quality filtering (Q ≥ 30) and a minimum read length of 100 bp. Amplicon sequence variants (ASVs) were inferred using DADA2. [52] Reads were filtered and trimmed per run, error models were learned, and ASVs were resolved. Sequence tables from separate runs were merged, chimeras removed, and taxonomy assigned using the SILVA database (v1.3.8). We used phyloseq to filter out non-bacterial ASVs and apply a prevalence filter of 5% and remaining sequences were used to calculate alpha and beta diversity (bray-curtis distances). Bray-curtis distances were ordinated using principal coordinate analysis (PCoA) and variance assessed using PERMANOVA.

Neonatal pulmonary gene expression analyses

RNA extraction and cDNA synthesis for quantitative PCR (qPCR)

Neonatal (P7) lung tissue was homogenized in TRIzol reagent (Life Technologies) and total RNA was isolated using chloroform–isopropanol phase separation and ethanol washes according to standard protocols. RNA was resuspended in ultrapure water and quality was evaluated using a NanoDrop 2000 spectrophotometer (Thermo Scientific, Waltham, MA, USA) with Nano Drop 2000/2000c software (Thermo Scientific). Following extraction, 2 µg of RNA was used for cDNA synthesis using the Superscript VILO™ cDNA Synthesis Kit (Life Technologies) in accordance with the manufacturer's instructions.

Quantitative PCR

To quantify transcript levels, quantitative real time PCR was performed using the LightCycler 480 II (Roche, Basel, Switzerland) and LightCycler 480 SYBR Green I Master (catalogue no. 04887352001; Roche). Sequences of primers used for qPCR are provided in Supplementary Table S2; all primers were obtained from Life Technologies. The PCR cycling conditions used for each assay were enzyme activation at 95°C for 5 min, amplification of the gene product through 40 successive cycles of 95°C for 10 s, 60°C for 10 s, and 72°C for 10 s. The specificity of each primer set was confirmed by melt curve analysis. qPCR was performed in triplicate for each sample using standard curves generated from pooled cDNA and crossing point (Cp) values were determined with LightCycler 480 software. The geometric mean of three housekeeping genes, tyrosine 3-monooxygenase/tryptophan 5-monooxygenase activation protein gamma (*Ywhag*) and hypoxanthine-guanine phosphoribosyltransferase (*Hpht*), and Beta-2-microglobulin (*B2m*) were used as reference gene values for each sample.

Intestinal histology

Offspring intestinal morphology was evaluated in ileum and colon tissue collected pre- and post-infection (P90 and P120). To assess intestinal villi lengths, crypt depths, and goblet cell counts, a 1 cm long tissue section of distal ileum and distal colon was collected and fixed for 3 hours at room temperature in Carnoy's fixative (6:3:1 ethanol: chloroform: glacial acetic acid), and stored in 70% ethanol until processing. Fixed tissues were processed using a Leica Biosystems processor (#TP1020) as follows: 70% ethanol (2x1 hour), 90% ethanol (2x1 hour), 100% ethanol (2x1 hour), Histoclear (Fisher Scientific, #50-329-50) (3x1 hour), and Leica Paraplast PLUS (Leica Biosystems, #39602004) (3x1 hour). Tissues were manually embedded in paraffin for cross-sectional analysis. Tissue sections of 4 µm were cut at 120 µm intervals per tissue sample on a Leica Microtome, incubated at 37°C overnight and stored until histological staining.

Mucin was stained in tissue sections using Alcian Blue (8 GX- Sigma Aldrich). Sections were deparaffinized, rehydrated, stained and cover slips mounted. Brightfield images were captured at 10x magnification using a Nikon Eclipse NI microscope and analyzed using ImageJ Software. Villus length and crypt depth were measured and averaged across 20 villi and 20 crypts per tissue section. Goblet cell counts per villus and crypt were averaged across 10 villi and 10 crypts per tissue section, in three to four tissue sections per mouse.

Statistical analyses

For all analyses in this study, the litter was considered a single biological replicate. Where littermates were used within a single analysis, data points were treated as repeated measures. Pre- and post-infection terminal measures (i.e., histological assessment of intestinal morphology and islets, as well as microbiota composition) were analyzed as cross-sectional comparisons between groups at each time point as these outcomes could not be measured longitudinally. Neonatal (P7) data were analyzed by two-way ANOVA with Bonferonni's *post-hoc* test in GraphPad Prism. All other measures were analyzed by mixed-effects linear models using the lmerTest package in R with diet, sex, and infection (where applicable) as fixed effects and litter as a random effect to nest repeated measures across littermates. For time-course experiments (i.e., *in vivo* intestinal permeability assays, OGTTs), mouse ID was included as an additional random effect to account for repeated measures within individual animals. Where significant main effects were present in linear models, pairwise post-hoc comparisons were made between the estimated marginal means using the emmeans package in R. For all analyses, $p < 0.05$ was used as a nominal threshold for determining statistical significance.

Results

Maternal and offspring general phenotyping

As we have previously shown, dams fed a HF diet were significantly (~ 30%) heavier (CTL 25.55g ± 5.71; mHF 31.26g ± 1.28, p = 0.0006), and had increased body fat (CTL 0.25 ± 0.38; mHF 0.64 ± 0.08, p =

0.0003) compared to CTL dams at weaning.[24] Overall, offspring born to mHF dams exhibited significant physiological differences compared to CTL offspring across a number of developmental time points. Neonates born to mHF mothers showed elevated body weights compared to CTL offspring at P7, P14, and P21 (Table 1), increased Lee Index, higher heart and spleen weights and decreased intestinal length at P7 compared to CTL offspring (Suplementary Table S3). After weaning at P21, mHF offspring weighed less than controls at 60 and 90 days of age but were not different at 120 days (Table 1). Offspring born to mHF had higher mesenteric fat mass and lower liver mass compared to CTL offspring; effects that were especially apparent in male mHF offspring (Suplementary Table S3). In addition to these systemic physiological differences, significant changes in neonatal lung tissue were also observed.

Table 1
Maternal excess adiposity is associated with weight changes in adult mice offspring.

Parameters	Male		Female		Statistical outcomes
	CTL	mHF	CTL	mHF	
P7 Body Mass (g)	3.72 ± 0.06	3.91 ± 0.10	3.62 ± 0.06	3.9 ± 0.10	DxS^{ns} / D* / S^{ns}
P14 Body Mass (g)	6.91 ± 0.10	7.7 ± 0.10	6.9 ± 0.11	7.68 ± 0.11	DxS^{ns} / D**** / S^{ns}
P21 Body Mass (g)	8.53 ± 0.12	10.52 ± 0.13	8.26 ± 0.14	10.25 ± 0.11	DxS^{ns} / D**** / S^{ns}
P60 Body Mass (g)	23.32 ± 0.26	22.58 ± 0.20	18.18 ± 0.10	17.85 ± 0.16	DxS^{ns} / D** / S****
P90 Body Mass (g)	26.45 ± 0.32	24.93 ± 0.86	20.65 ± 0.35	18.25 ± 0.99	DxS^{ns} / D* / S****
P120 Body Mass (g)	26.55 ± 0.56	24.75 ± 1.11	19.91 ± 0.41	18.72 ± 1.31	DxS^{ns} / D^{ns}/ S****
CNT - CFU (Log10)	4.82 ± 0.13	5.03 ± 0.18	4.42 ± 0.21	4.55 ± 0.09	DxS^{ns} / D^{ns}/ S*

Data are expressed as Mean ± SEM. Control (CTL), Maternal high-fat (mHFD). CTL-M (n = 8–21) mHF-M (n = 9–31), CTL-F (n = 7–21), and mHF-F (6–28). Interaction between diet and sex factors (DxS); diet factor (D), and sex factor (S); *p < 0.05, **p < 0.01, ***p < 0.001, ****p < 0.0001 and ns. Central nasal turbinate (CNT), Colony Forming Units (CFU), grip force (gf), and non-significant (ns).

Inflammation-associated gene transcripts are increased in mHF neonatal lungs

To investigate whether neonates born to mHF dams were destined for poor lung responses, we investigated key genes involved in pulmonary immune and structural homeostasis that are mechanistically linked to pneumococcal susceptibility. Specifically, we assessed expression of the

platelet-activating factor receptor (*Ptafr*),[53] a known receptor facilitating pneumococcal adherence; the pattern recognition receptors *Tlr2* and *Tlr4*,[54,55] which are critical for bacterial sensing and innate immune activation; surfactant proteins (*Sftpa, Sftpb, Sftpc*),[56,57] which function as pulmonary opsonins and contribute to host defense; and *Pcyt1a*, an essential regulator of surfactant phospholipid synthesis and alveolar structural integrity.[58]

At postnatal day 7 (P7), neonates born to mHF dams displayed elevated transcript levels of platelet-activating factor receptor (*Ptafr*), Toll-like receptor 2 (*Tlr2*), and Toll-like receptor 4 (*Tlr4*) in lung tissue compared to CTL neonates (Fig. 2). These increases were accompanied by a reduction in transcript levels of surfactant signalling factors, including surfactant protein A (*SftpA*), surfactant protein B (*SftpB*), and surfactant protein C (*SftpC*). Transcript levels of phosphate cytidylyltransferase 1A (*Pcyt1a*), a rate limiting enzyme of phosphatidylcholine (PC) synthesis were also reduced (Fig. 2). These effects were sex-dependant; multiple comparison analyses revealed that these changes in transcript levels were predominantly observed in male mHF neonates (Fig. 2).

Offspring immunophenotype is impacted by mHF in a sex dependant manner

Consistent with our previous work,[59] proportions of circulating neutrophils and monocytes were generally higher in preinfection at ~P90 in male offspring compared to females (Supplementary Figure S1c-d) ; p_{sex} = 0.0033 and 0.042, respectively). This increased proportion of monocytes was primarily due to an increased proportion of inflammatory (Ly6C^{hi}) monocytes (Supplementary Figure S1d). Females, in contrast to males, exhibited a lymphoid shift in the composition of circulating leukocytes (p_{sex} = 0.002). We found no significant impact of maternal diet on the composition of peripheral blood leukocyte populations (% of CD45^{+}) in male or female offspring at ~P90 (pre-infection; Supplementary Figure S1). Even though the proportion of leukocytes did not change however, the absolute numbers of leukocytes were reduced in both male and female mHF compared to CTL offspring (p_{diet} <0.001; Fig. 3a).

In turn, populations of most major leukocyte lineages were also reduced in mHF offspring. Both sexes exhibited a pronounced drop in the number of circulating lymphocytes (p_{diet} <0.001; Fig. 3b) and reduced neutrophil counts were more pronounced in male mHF offspring (Fig. 3c). Similar trends were observed for monocyte populations, with total monocytes and constituent Ly6C^{hi} and Ly6C^{low} subtypes being reduced in mHF male offspring only (Fig. 3d – e). Ly6C^{neg} monocytes were reduced irrespective of offspring sex (Fig. 3e). Within the monocyte population, male mHF offspring exhibited an increased proportion of Ly6C^{low} monocytes at the expense of reduced Ly6C^{hi} monocyte frequency. We also observed a sex-dependent effect of mHF exposure on Ly6C^{neg} monocytes ($p_{Int.}$ = 0.022), with their frequency within the total monocyte dropping in females but increasing in males, although this effect did not reach statistical significance in post-hoc pairwise comparisons (Supplementary Figure S2). The impact of mHF diet on offspring monocyte-to-lymphocyte ratio was also sex-dependent, decreasing in

male but not female offspring (p_{int} = 0.015). Neutrophil to lymphocyte ratio was unaffected by mHF diet exposure (Supplementary Figure S3). Together, these findings suggest that mHF exposure alters the pre-infection circulating immune profile in a sex-dependent manner, potentially impairing offspring immune responses following respiratory challenge.

Pneumococcal challenge modifies the impact of mHF on offspring peripheral immunophenotype

At 90 days of age, we challenged offspring with a low (10^4 colony-forming units; CFUs) intranasal dose of *S. pneumoniae*. This dose was selected to induce a robust colonization which was confirmed in a subset of animals, three days post infection (P93), where we confirmed that offspring carried levels of *S. pneumoniae* in the nasal turbinates at rates that were similar between groups (Table 1) although females generally had lower CFUs than males. At sacrifice (30 days post infection), the majority of mice had cleared colonization, consistent with previously reported studies.[60] Thus, maternal high-fat diet exposure did not impair primary pneumococcal colonization in this sub-lethal challenge model. We therefore interpreted subsequent intestinal, immune, microbial, and metabolic changes as an alteration to post-challenge resilience rather than as consequences of acute bacterial burden.

At ~ 30 days after *S. pneumoniae* infection (P120; Fig. 4 and Supplementary Fig. 4), the proportional composition of peripheral blood leukocyte frequencies remained similar between CTL and mHF offspring (Supplementary Fig. 4). While $Ly6C^{low}$ monocytes remained elevated in male and female mHF offspring, the magnitude of the increase was significant only in females (Supplementary Fig. 5). No differences in either monocyte-to-lymphocyte or neutrophil-to-lymphocyte ratios were observed between groups (Supplementary Fig. 6). Thus, the previously observed mHF-induced changes in absolute quantities of lymphocytes, neutrophils, and monocytes at ~P90 were no longer present post-infection challenge (Fig. 4).

Pneumococcal challenge reveals impaired intestinal barrier function, altered gut ultrastructure, and shifts microbiome composition in offspring

To understand whether maternal diet-induced excess adiposity and alters offspring intestinal permeability after postnatal *S. pneumoniae* challenge, we measured serum fluorescence levels following oral FITC-dextran gavage, at both pre-infection (~ P90) and post-infection (P120) timepoints (Fig. 5). While *S. pneumoniae* challenge had little effect on intestinal permeability in CTL offspring, it significantly impaired intestinal permeability in both male and female mHF offspring (pairwise, $p < 0.05$, Fig. 5a,c). Areas under the curve of fluorescence levels over time confirmed that *S. pneumoniae* exposure induced higher permeability over time in mHF offspring compared to CTL offspring in both males and females (p_{inf} = 7e-05, $p_{dietxinf}$ = 0.0103 and pairwise $p < 0.05$ post- vs. pre-infection, Fig. 5b,d). These data suggest that exposure to mHF in early life results in impaired intestinal permeability after a postnatal infection challenge.

We further investigated whether this impaired post-infection intestinal permeability was associated with altered intestinal morphology by measuring villus length and crypt depth in the ileum and colon. The analyses were performed in both pre- and post-infection offspring samples, but because intestinal tissue collection required euthanasia, pre- and post-infection samples were obtained from separate littermate offspring derived from the same dam. Tissues were collected at the experimental endpoint prior to infection, and 30 days post-infection. This design allowed biological replication while controlling for maternal and litter effects.

Maternal diet (p_{diet} = 0.0024) and *S. pneumoniae* challenge (p_{inf} = 0.0004) both had a significant effect on villus length (Fig. 6a, Fig. 7). The effect of *S. pneumoniae* was dependent on maternal diet ($p_{diet x inf}$ = 0.0422); where villus length was significantly reduced by infection challenge in CTL males and females, but not in mHF offspring. Similarly, crypt depths were impacted by both maternal diet (p_{diet} = 0.0331) and infection (p_{inf} = 0.0007). This was driven mostly by an effect in males rather than females (p_{sex} = 0.0030); infection challenge resulted in decreased crypt depths in mHF males (pairwise, $p < 0.05$) and CTL offspring, though this difference was not statistically significant (pairwise, p = 0.055) (Fig. 6b, 7). In the colon, infection (p_{inf} = 0.0308, Fig. 6e, 7) had a significant effect on crypt depths, driven by male CTL offspring (pairwise, $p < 0.05$). These data suggest that CTL offspring have intestinal morphology adaptations in response to infection that are not present in mHF offspring, which were particularly evident in the ileum.

In addition to intestinal ultrastructure, we also investigated the effects of maternal diet and *S. pneumoniae* challenge on offspring intestinal mucus production capacity by measuring goblet cell number in offspring ileum and colon at both pre-infection (~ P90) and post-infection (P120) timepoints (Fig. 6c-f, Fig. 7). Ileal villus goblet cell counts were reduced in mHF offspring (p_{diet}= 0.0257) with no effect of *S. pneumoniae*, and these effects were sex dependent (p_{sex} = 0.016, Fig. 6c, Fig. 7). Ileum crypt goblet cells counts were similar between groups (Fig. 6d, Fig. 7). In the colon, infection challenge had a significant effect on crypt goblet cell counts (p_{inf} = 0.0364), particularly in female CTL offspring (pairwise, $p < 0.05$, Fig. 6f, Fig. 7). These results suggest that the effect of infection challenge on mHF offspring intestinal function is likely not dependent on mucus production in either the ileum or colon, though there were effects of infection challenge observed in CTL but not mHF mice.

We next investigated whether intestinal microbial composition was impacted by maternal diet and offspring infection challenge (Supplemental Fig. 8). Thirty days post-infection, offspring demonstrated an altered microbial community composition relative to pre-infection baseline levels (Bray-Curtis dissimilarity; PERMANOVA; R^2 = 0.052, p = 0.0004), with a marginal effect of maternal diet (R^2 = 0.023, p = 0.055). Stratification by sex revealed that the infection effect was primarily driven by female offspring, where composition significantly differed between pre- and post-infection states, explaining10% of the variance in microbial composition (R^2 = 0.10, p = 0.0006). In contrast, male offspring showed no significant effects of infection challenge (p = 0.090) or diet (p = 0.49) on microbial beta-diversity,

suggesting an interactive effect of maternal diet on beta diversity that is dependant upon the sex of the offspring.

Glucose homeostasis is altered by mHF and S. pneumoniae challenge in offspring

Since the intestine is known to influence systemic metabolic homeostasis, we also investigated offspring glucose tolerance and insulin levels (Supplementary Fig. 9). We saw that *S. pneumoniae* challenge significantly impacted glucose tolerance (p_{inf}=0.0479), particularly in mHF offspring ($p_{dietxinf}$ = 0.0002) in a sex-specific manner (p_{sex} = 2.235e-06) (Supplemental Fig. 9a). While infection challenge had little effect on glucose tolerance in CTL offspring, it significantly altered glucose tolerence in both male and female mHF offspring. Areas under the curve values confirmed that infection challenge was associated with lower blood glucose responses in mHF offspring compared to CTL offspring, regardless of sex (p_{inf} = 0.0478, $p_{dietxinf}$ = 0.0002, p_{sex} = 0.4035). Infection also influenced serum insulin levels (p_{inf}=0.0286), where female mHF offspring had lower serum insulin levels after infection compared to pre-infection, without impacts in CTL offspring (Supplementary Fig. 9c). The ratio of glucose to insulin was similarly altered by *S. pneumoniae* challenge ($p_{Inf.}$ = 4e-05), whereas the insulin-to-glucose ratio was significantly higher in all offspring regardless of diet or sex (Supplementary Fig. 10). These findings suggest that the postnatal infection challenge contributed to significant changes in responses to oral glucose bolus in both control and mHF offspring.

Discussion

Epidemiological and experimental evidence links maternal excess adiposity to increased offspring risk of asthma, infection, and metabolic disease. Population-based studies show maternal body mass index is positively associated with increased rates of respiratory tract infections, wheeze, and asthma in children.[61–63] Mechanistically, maternal excess adiposity/obesity creates a chronic low-grade inflammatory in utero environment,[26,64,65] characterized by elevated TNF, IL-6, and altered TLR signaling. We have shown that HF diets impair maternal intestinal barrier function and alter peripheral immune cell composition in dams,[24,25] potentially increasing maternal–fetal exposure to inflammatory cytokines, microbial-derived products, and other immune mediators. These in utero inflammatory exposures may prime the fetal immune system leading to the dysregulation of lung,[66,67] and gut [68] development and combined, these changes may influence responses to infection challenge. Our neonatal findings of increased trancripts of pulmonary innate immune receptors and reduced surfactant markers align with this, suggesting that maternal adiposity could prime the developing lung for maladaptive responses to postnatal pathogen challenge.[66] Reduced expression of surfactant protein transcripts (*Sftpa–c*) in neonatal lungs may contribute to impaired alveolar surface tension regulation and innate lung immunity.[69] This is consistent with previous work that HFD-exposed fetal mice had delayed structural lung development, reduced cellular proliferation, and reduced *SpB*, *SpC*, and *SpD* gene expression levels compared with control fetuses.[41]

The use of a postnatal *S. pneumoniae* challenge allowed us to probe whether in utero immune programming would alter offspring response to a respiratory infection.[70] Mechanistically, prenatal inflammatory and metabolic stress has been shown to disrupt hematopoietic stem and progenitor cell (HSC) function, leading to altered myelopoiesis and downstream defects in monocyte/macrophage development and function.[71] Maternal high-fat diet exposure induces pro-inflammatory programming and altered HSC differentiation in fetal hematopoietic progenitors in nonhuman primates, while experimental prenatal inflammation leads to persistent changes in HSC function and postnatal immune output in murine models.[72] This aligns with work showing that prenatal inflammation disrupts myelopoiesis[73,74] and monocyte/macrophage function,[75] and models showing maternal obesity reduces fetal hematopoietic stem cell output.[71] In our model, while maternal HF diet altered the baseline myeloid landscape, it did not result in significant differences in survival or overall infection severity following *S. pneumoniae* challenge. This stands in contrast to neonatal rat models of viral infection, where offspring from HF-fed dams displayed heightened proinflammatory cytokine expression in lung tissues and were more susceptible to severe respiratory syncytial virus (RSV) five days after infection.[71] While we observed shifts in monocyte subsets, the lack of differential mortality in our study suggests that the developmental programming effects of a maternal excess adiposity may manifest differently in bacterial versus viral respiratory challenges. Furthermore, while total deficiency in receptors like CCR2 is known to impair monocyte migration and lead to recurrent infections in humans,[76] our findings suggest that the more subtle, adiposity-induced shifts in myeloid composition we observed were not sufficient to compromise the primary clearance of a sub-lethal bacterial challenge. Thus, the major phenotype identified was not increased acute susceptibility to pneumococcal infection, but reduced multisystem resilience following respiratory challenge.

The role of the gut–lung axis has gained increasing attention as a bidirectional pathway influencing both local and systemic immune responses. [77] Altered gut microbiota composition and increased intestinal permeability can potentiate lung inflammation through the translocation of microbial products and systemic cytokine release. [78,79] Maternal excess adiposity may disrupt this balance, predisposing offspring to respiratory complications. In our study, maternal excess adiposity and postnatal infection together altered gut microbial diversity and beta dispersion, particularly in female offspring, suggesting sex-dependent shifts in microbial resilience. Given that microbiota-derived metabolites such as short-chain fatty acids regulate both gut and lung immunity,[80–82] these shifts may further compound later life immune vulnerability. The finding that females exhibited greater post-infection changes in microbiota composition suggests a less stable response to challenges like *S. pneumoniae* infection, which could predispose to chronic inflammation or impaired recovery.

Our data implicate the gut as a critical site of postnatal vulnerability, particularly in the context of infectious challenges. We and others have shown that maternal obesity changes microbial gut composition[83–85] and increases intestinal permeability.[86] Our current findings show that maternal HF diet-induced excess adiposity decreased intestinal length in neonates, altered glucose profiles, and impaired intestinal permeability in adult offspring after an infection challenge. Indeed, *S. pneumoniae*

challenge unmasked barrier dysfunction in mHF offspring; the result of a two-hit interaction between prenatal exposure and postnatal challenge. This supports prior work showing that early-life insults could sensitize intestinal tissues to later inflammatory triggers.[73,74] Structurally, shortened villi, decreased crypt depth, and reduced goblet cell numbers in the ileum and colon suggest compromised mucosal integrity and mucus barrier function, critical for pathogen exclusion and immune regulation. Goblet cells modulate innate immunity[87] by producing mucins and antimicrobial peptides. Disruption of these processes may impair antigen sampling and tolerance induction, increasing susceptibility to dysbiosis and infection. These observations align with findings that disruptions in gut microbiota and mucosal immunity contribute to heightened infection risk.[23,88] Whether pulmonary goblet cells are similarly affected was beyond the scope of the current study but would be useful to investigate in future work.

In addition to immune and intestinal effects, we observed that *S. pneumoniae* challenge unmasked changes in offspring glucose homeostasis. While baseline glucose tolerance was only mildly impaired in mHF offspring, post-infection glucose clearance was paradoxically improved, especially in females. Although counterintuitive, this may reflect an increased need for glucose uptake by activated immune cells or infection-induced metabolic reprogramming.[89] This cellular metabolic demand likely operates within a broader systemic context; indeed, recent work shows that adiposity and hyperinsulinemia in offspring resulting from maternal diet-induced obesity precede airway hyperresponsiveness in later life,[10] which was not present in early life but emerged later with increased adiposity and hyperinsulinemia.[9] Together, these findings support the idea that maternal excess adiposity programs metabolic-immune flexibility, such that a respirctory infection can produce persistent effects beyond the lung.

Together, our findings support a multi-organ, sex-dependent reprogramming where maternal excess adiposity sets the stage for altered responses to postnatal environmental challenges, including infection. This work builds on previous studies linking maternal excess adiposity to postnatal health, early lung and gut development, and postnatal immune-metabolic outcomes. We recognize however, that this study is not without limitations. While reduced surfactant gene expression and increased innate immune transcripts are suggestive of impaired lung defense capacity we did not perform functional studies to determine whether these transcript-level changes are causal or correlative. While peripheral blood immunophenotyping provides insight into systemic immune capacity it does not speak to lung-resident or gut-resident immune cell responses. Finally, because we did not observe increased acute pneumococcal burden and did not directly assess lung-resident immune responses, pulmonary tissue repair, or inflammatory resolution, we cannot conclude that maternal adiposity impairs primary antibacterial defence. Instead, our data support a model in which maternal adiposity reduces offspring resilience to inflammatory challenge across intestinal, immune, microbial, and metabolic systems.

In conclusion, we show that maternal excess adiposity alters offspring developmental trajectories in a manner that increases infection-induced secondary immune, intestinal, and metabolic dysregulation later in life. These effects were evident in neonatal pulmonary immune-developmental markers, baseline

circulating immune profiles, and post-challenge intestinal barrier, microbial, and glucose–insulin outcomes. Together, these findings support a developmental programming model in which maternal adiposity establishes latent intestinal–immune–metabolic vulnerabilities that become apparent after later-life inflammatory stress. Given the increasing prevalence of periconception excess adiposity, understanding underlying mechanisms is crucial for developing targeted interventions to mitigate the intergenerational transmission of metabolic and immune disorders and vulnerability to infection.

Declarations

Conflicts of interest

There are no conflicts of interest for any of the authors.

Ethical standards

All animal procedures were approved by the Animal Ethics Research Board at McMaster University (Animal Utilization Protocol 24–27, 21-04-13) in accordance with the Canadian Council of Animal Care guidelines.

Footnotes

Tatiane A. Ribeiro and Anastasia Warmington are co-first authors

Funding

declaration

This work was funded by a team grant from the Canadian Institutes of Health Research (CIHR) Geroscience grant (GER-163047) and the Lung Health Foundation. TAR was supported by a McMaster Institute for Research on Aging Postdoctoral Fellowship and a Michael G. DeGroote Fellowship Award. AW was supported by a CIHR Fredrick Banting and Charles Best Canadian Graduate Scholarship. JAB was supported by a Queen Elizabeth II Graduate Scholarship in Science and Technology (QEII-GSST). DMS is supported by the Canada Research Chairs Program.

Author Contribution

TAR, AW, DMS, and DMEB designed the study; TAR, BKEK, and BC generated the in vivo animal data. TAR, AW, EY, CJB, BKEK, PAJ, JAB, ED, and JS, performed the experiments. AW and BC performed the S. pneumoniae infections. JS, JAB, AW, and ED immunophenotyping. TAR, EY, KK, and CJB analyzed and

interpreted the data. TAR and DMS wrote the manuscript. MM performed the gut histology. TAR, AW, EY, KK, CJB, BBEK, BC, PAJ, JAB, ED, JS, MM, AL, DMEB, and DMS contributed with critical revision of the manuscript for important intellectual content. DMEB and DMS supervised and received funding for the project development.

Acknowledgement

We would like to thank the McMaster University Central Animal Facility for their care of the animals.

Data Availability

The raw 16S amplicon sequencing data are deposited in the European Nucleotide Archive under accession number PRJEB113405.

References

1. Althaus, T. et al. Associations between maternal obesity and infectious morbidity in Zimbabwean infants. *Eur. J. Clin. Nutr.* **76**, 328–333. https://doi.org/10.1038/s41430-021-00907-4 (2022).
2. Driscoll, A. K. & Gregory, E. C. W. Increases in Prepregnancy Obesity: United States, 2016–2019. *NCHS Data Brief*, 1–8 (2020).
3. Nurul-Farehah, S. & Rohana, A. J. Maternal obesity and its determinants: A neglected issue? *Malays Fam Physician*. **15**, 34–42 (2020).
4. Bellissimo, C. J., Beristain, A. G. & Sloboda, D. M. Impacts of maternal excess adiposity on the uterine immune environment: contributions to placental dysfunction and adverse pregnancy outcomes. *Reproduction* https://doi.org/10.1530/rep-24-0464 (2025).
5. Fowden, A. L., Camm, E. J. & Sferruzzi-Perri, A. N. Effects of Maternal Obesity On Placental Phenotype. *Curr. Vasc Pharmacol.* **19**, 113–131. https://doi.org/10.2174/1570161118666200513115316 (2021).
6. Kislal, S., Shook, L. L. & Edlow, A. G. Perinatal exposure to maternal obesity: Lasting cardiometabolic impact on offspring. *Prenat Diagn.* **40**, 1109–1125. https://doi.org/10.1002/pd.5784 (2020).
7. Kankowski, L. et al. The Impact of Maternal Obesity on Offspring Cardiovascular Health: A Systematic Literature Review. *Front. Endocrinol. (Lausanne)*. **13**, 868441. https://doi.org/10.3389/fendo.2022.868441 (2022).
8. Menting, M. D. et al. Maternal obesity in pregnancy impacts offspring cardiometabolic health: Systematic review and meta-analysis of animal studies. *Obes. Rev.* **20**, 675–685. https://doi.org/10.1111/obr.12817 (2019).
9. Williams, K. R., Bright, H. A., Fryer, A. D., Jacoby, D. B. & Nie, Z. Maternal high-fat diet programs offspring airway hyperinnervation and hyperresponsiveness. *JCI Insight*. **10**

https://doi.org/10.1172/jci.insight.181070 (2025).

10. Calco, G. N. et al. Maternal high-fat diet increases airway sensory innervation and reflex bronchoconstriction in adult offspring. *Am. J. Physiol. Lung Cell. Mol. Physiol.* **325**, L66–l73. https://doi.org/10.1152/ajplung.00115.2023 (2023).
11. Curren, B. et al. A maternal high-fat diet predisposes to infant lung disease via increased neutrophil-mediated IL-6 trans-signaling. *Cell. Rep.* **43**, 114974. https://doi.org/10.1016/j.celrep.2024.114974 (2024).
12. Dixon, A. E. & Peters, U. The effect of obesity on lung function. *Expert Rev. Respir Med.* **12**, 755–767. https://doi.org/10.1080/17476348.2018.1506331 (2018).
13. MacDonald, K. D., Moran, A. R., Scherman, A. J., McEvoy, C. T. & Platteau, A. S. Maternal high-fat diet in mice leads to innate airway hyperresponsiveness in the adult offspring. *Physiol. Rep.* **5** https://doi.org/10.14814/phy2.13082 (2017).
14. Berger, M., Geng, B., Cameron, D. W., Murphy, L. M. & Schulman, E. S. Primary immune deficiency diseases as unrecognized causes of chronic respiratory disease. *Respir Med.* **132**, 181–188. https://doi.org/10.1016/j.rmed.2017.10.016 (2017).
15. Forno, E., Young, O. M., Kumar, R., Simhan, H. & Celedón, J. C. Maternal obesity in pregnancy, gestational weight gain, and risk of childhood asthma. *Pediatrics* **134**, e535–546. https://doi.org/10.1542/peds.2014-0439 (2014).
16. Halonen, M. et al. Perinatal tumor necrosis factor-α production, influenced by maternal pregnancy weight gain, predicts childhood asthma. *Am. J. Respir Crit. Care Med.* **188**, 35–41. https://doi.org/10.1164/rccm.201207-1265OC (2013).
17. Liu, S. et al. Pre-pregnancy Maternal Weight and Gestational Weight Gain Increase the Risk for Childhood Asthma and Wheeze: An Updated Meta-Analysis. *Front. Pediatr.* **8**, 134. https://doi.org/10.3389/fped.2020.00134 (2020).
18. Rose, D. R. et al. Long-term altered immune responses following fetal priming in a non-human primate model of maternal immune activation. *Brain Behav. Immun.* **63**, 60–70. https://doi.org/10.1016/j.bbi.2016.11.020 (2017).
19. RR, E. L., Teixeira, C. J., Bordin, S., Antunes, E. & Anhe, G. F. Maternal Obesity in Mice Exacerbates the Allergic Inflammatory Response in the Airways of Male Offspring. *Nutrients* **11** https://doi.org/10.3390/nu11122902 (2019).
20. Samarasinghe, T. D. et al. The effect of prenatal maternal infection on respiratory function in mouse offspring: evidence for enhanced chemosensitivity. *J. Appl. Physiol. (1985)*. **119**, 299–307. https://doi.org/10.1152/japplphysiol.01105.2014 (2015).
21. Ghigliotti, G. et al. Adipose tissue immune response: novel triggers and consequences for chronic inflammatory conditions. *Inflammation* **37**, 1337–1353. https://doi.org/10.1007/s10753-014-9914-1 (2014).
22. Selle, J. et al. Maternal and perinatal obesity induce bronchial obstruction and pulmonary hypertension via IL-6-FoxO1-axis in later life. *Nat. Commun.* **13**, 4352.

https://doi.org/10.1038/s41467-022-31655-z (2022).

23. Xue, Y., Wang, H., Du, M. & Zhu, M. J. Maternal obesity induces gut inflammation and impairs gut epithelial barrier function in nonobese diabetic mice. *J. Nutr. Biochem.* **25**, 758–764. https://doi.org/10.1016/j.jnutbio.2014.03.009 (2014).
24. Breznik, J. A. et al. Maternal adaptations in mouse lactation are vulnerable to diet-induced excess adiposity. *bioRxiv*, 2006. 2030.547298 (2023). (2023).
25. Ribeiro, T. A. et al. Intestinal permeability and peripheral immune cell composition are altered by pregnancy and adiposity at mid- and late-gestation in the mouse. *PLoS One*. **18**, e0284972. https://doi.org/10.1371/journal.pone.0284972 (2023).
26. Gohir, W. et al. High-fat diet intake modulates maternal intestinal adaptations to pregnancy and results in placental hypoxia, as well as altered fetal gut barrier proteins and immune markers. *J. Physiol.* **597**, 3029–3051 (2019).
27. Fulde, M. & Hornef, M. W. Maturation of the enteric mucosal innate immune system during the postnatal period. *Immunol. Rev.* **260**, 21–34 (2014).
28. Pantazi, A. C. et al. Development of Gut Microbiota in the First 1000 Days after Birth and Potential Interventions. *Nutrients* **15** https://doi.org/10.3390/nu15163647 (2023).
29. Renz, H., Brandtzaeg, P. & Hornef, M. The impact of perinatal immune development on mucosal homeostasis and chronic inflammation. *Nat. Rev. Immunol.* **12**, 9–23 (2012).
30. Mulligan, C. M. & Friedman, J. E. Maternal modifiers of the infant gut microbiota: metabolic consequences. *J. Endocrinol.* **235**, R1–r12. https://doi.org/10.1530/joe-17-0303 (2017).
31. Selma-Royo, M. et al. Perinatal environment shapes microbiota colonization and infant growth: impact on host response and intestinal function. *Microbiome* **8**, 1–19 (2020).
32. Arrieta, M. C. et al. Early infancy microbial and metabolic alterations affect risk of childhood asthma. *Sci. Transl Med.* **7**, 307ra152. https://doi.org/10.1126/scitranslmed.aab2271 (2015).
33. Piersigilli, F., Van Grambezen, B., Hocq, C. & Danhaive, O. Nutrients and Microbiota in Lung Diseases of Prematurity: The Placenta-Gut-Lung Triangle. *Nutrients* 12 (2020). https://doi.org/10.3390/nu12020469
34. Arslan, S., Yıldıran, H. & Seymen, C. M. The Effect of Maternal High-Fat Diet on Adipose Tissue Histology and Lipid Metabolism-Related Genes Expression in Offspring Rats. *Nutrients* **16** https://doi.org/10.3390/nu16010150 (2024).
35. Coley, E. J. L. et al. Early life adversity predicts brain-gut alterations associated with increased stress and mood. *Neurobiol. Stress*. **15**, 100348. https://doi.org/10.1016/j.ynstr.2021.100348 (2021).
36. Enaud, R. et al. The Gut-Lung Axis in Health and Respiratory Diseases: A Place for Inter-Organ and Inter-Kingdom Crosstalks. *Front. Cell. Infect. Microbiol.* **10**, 9. https://doi.org/10.3389/fcimb.2020.00009 (2020).
37. Liu, X. et al. High-fiber diet mitigates maternal obesity-induced cognitive and social dysfunction in the offspring via gut-brain axis. *Cell. Metab.* **33**, 923–938e926.

https://doi.org/10.1016/j.cmet.2021.02.002 (2021).

38. Ribaroff, G. A., Wastnedge, E., Drake, A. J., Sharpe, R. M. & Chambers, T. J. G. Animal models of maternal high fat diet exposure and effects on metabolism in offspring: a meta-regression analysis. *Obes. Rev.* **18**, 673–686. https://doi.org/10.1111/obr.12524 (2017).
39. Dickson, R. P., Erb-Downward, J. R., Martinez, F. J. & Huffnagle, G. B. The Microbiome and the Respiratory Tract. *Annu. Rev. Physiol.* **78**, 481–504. https://doi.org/10.1146/annurev-physiol-021115-105238 (2016).
40. Dickson, R. P. et al. Enrichment of the lung microbiome with gut bacteria in sepsis and the acute respiratory distress syndrome. *Nat. Microbiol.* **1**, 16113. https://doi.org/10.1038/nmicrobiol.2016.113 (2016).
41. Mayor, R. S. et al. Maternal high-fat diet is associated with impaired fetal lung development. *Am. J. Physiol. Lung Cell. Mol. Physiol.* **309**, L360–368. https://doi.org/10.1152/ajplung.00105.2015 (2015).
42. Bolton, J. L., Auten, R. L. & Bilbo, S. D. Prenatal air pollution exposure induces sexually dimorphic fetal programming of metabolic and neuroinflammatory outcomes in adult offspring. *Brain Behav. Immun.* **37**, 30–44. https://doi.org/10.1016/j.bbi.2013.10.029 (2014).
43. Entringer, S. et al. Influence of prenatal psychosocial stress on cytokine production in adult women. *Dev. Psychobiol.* **50**, 579–587. https://doi.org/10.1002/dev.20316 (2008).
44. Kuhlman, K. R. Pitfalls and potential: Translating the two-hit model of early life stress from pre-clinical non-human experiments to human samples. *Brain Behav. Immun. Health*. **35**, 100711. https://doi.org/10.1016/j.bbih.2023.100711 (2024).
45. Bellissimo, C. J. et al. Maternal high-fat, high-sucrose diet-induced excess adiposity is linked to placental hypoxia and disruption of fetoplacental immune homeostasis in late gestation. *Biology Reproduction*, ioaf143 (2025).
46. Bernardis, L. L. & Patterson, B. D. Correlation between 'Lee index' and carcass fat content in weanling and adult female rats with hypothalamic lesions. *J. Endocrinol.* **40**, 527–528. https://doi.org/10.1677/joe.0.0400527 (1968).
47. Puchta, A., Verschoor, C. P., Thurn, T. & Bowdish, D. M. Characterization of inflammatory responses during intranasal colonization with Streptococcus pneumoniae. *J Vis Exp*, e50490 (2014). https://doi.org/10.3791/50490
48. Puchta, A. et al. TNF Drives Monocyte Dysfunction with Age and Results in Impaired Anti-pneumococcal Immunity. *PLoS Pathog*. **12**, e1005368. https://doi.org/10.1371/journal.ppat.1005368 (2016).
49. Ashburn, D. D., DeAntonio, A. & Reed, M. J. Pulmonary system and obesity. *Crit. Care Clin.* **26**, 597–602. https://doi.org/10.1016/j.ccc.2010.06.008 (2010).
50. Kennedy, K. M. et al. Parity modulates impact of BMI and gestational weight gain on gut microbiota in human pregnancy. *Gut Microbes*. **15**, 2259316. https://doi.org/10.1080/19490976.2023.2259316 (2023).

51. Whelan, F. J. et al. Culture-enriched metagenomic sequencing enables in-depth profiling of the cystic fibrosis lung microbiota. *Nat. Microbiol.* **5**, 379–390. https://doi.org/10.1038/s41564-019-0643-y (2020).
52. Stegmann, S. K. et al. Perinatal obesity primes the hepatic metabolic stress response in the offspring across life span. *Sci. Rep.* **15**, 6416. https://doi.org/10.1038/s41598-025-90082-4 (2025).
53. Rijneveld, A. W. et al. Improved host defense against pneumococcal pneumonia in platelet-activating factor receptor-deficient mice. *J. Infect. Dis.* **189**, 711–716. https://doi.org/10.1086/381392 (2004).
54. Dessing, M. C., Florquin, S., Paton, J. C. & van der Poll, T. Toll-like receptor 2 contributes to antibacterial defence against pneumolysin-deficient pneumococci. *Cell. Microbiol.* **10**, 237–246. https://doi.org/10.1111/j.1462-5822.2007.01035.x (2008).
55. Malley, R. et al. Recognition of pneumolysin by Toll-like receptor 4 confers resistance to pneumococcal infection. *Proc. Natl. Acad. Sci. U S A*. **100**, 1966–1971. https://doi.org/10.1073/pnas.0435928100 (2003).
56. Crouch, E., Hartshorn, K. & Ofek, I. Collectins and pulmonary innate immunity. *Immunol. Rev.* **173**, 52–65. https://doi.org/10.1034/j.1600-065x.2000.917311.x (2000).
57. Whitsett, J. A. Surfactant proteins in innate host defense of the lung. *Biol. Neonate*. **88**, 175–180. https://doi.org/10.1159/000087580 (2005).
58. Tian, Y., Zhou, R., Rehg, J. E. & Jackowski, S. Role of phosphocholine cytidylyltransferase alpha in lung development. *Mol. Cell. Biol.* **27**, 975–982. https://doi.org/10.1128/mcb.01512-06 (2007).
59. Breznik, J. A. et al. Effects of Obesity-Associated Chronic Inflammation on Peripheral Blood Immunophenotype Are Not Mediated by TNF in Female C57BL/6J Mice. *ImmunoHorizons* 5, 370–383 (2021).
60. Nelson, A. L. et al. Capsule enhances pneumococcal colonization by limiting mucus-mediated clearance. *Infect. Immun.* **75**, 83–90. https://doi.org/10.1128/iai.01475-06 (2007).
61. Rajappan, A. et al. Maternal body mass index: Relation with infant respiratory symptoms and infections. *Pediatr. Pulmonol.* **52**, 1291–1299. https://doi.org/10.1002/ppul.23779 (2017).
62. Videholm, S., Silfverdal, S. A. & Reniers, G. Maternal weight and infections in early childhood: a cohort study. *Arch. Dis. Child.* **104**, 58–63. https://doi.org/10.1136/archdischild-2017-314628 (2019).
63. Warmington, A. V., Bowdish, D. M. E., Sherifali, D. & Sloboda, D. M. A Scoping Review of the Relationship Between Maternal BMI and Offspring Incidence of Respiratory Infection: Where Do We Go From Here? *AJPM Focus*. **3**, 100234. https://doi.org/10.1016/j.focus.2024.100234 (2024).
64. Rees, A., Richards, O., Allen-Kormylo, A., Jones, N. & Thornton, C. A. Maternal body mass index is associated with an altered immunological profile at 28 weeks of gestation. *Clin. Exp. Immunol.* **208**, 114–128. https://doi.org/10.1093/cei/uxac023 (2022).
65. Saucedo, R. et al. Gestational Weight Gain Is Associated with the Expression of Genes Involved in Inflammation in Maternal Visceral Adipose Tissue and Offspring Anthropometric Measures. *J. Clin. Med.* **12** https://doi.org/10.3390/jcm12216766 (2023).

66. Losol, P. et al. Maternal high-fat diet in mice alters immune regulation and lung function in the offspring. *Br. J. Nutr.* **126**, 844–852. https://doi.org/10.1017/s0007114520004742 (2021).
67. Nguyen, D. N. et al. Prenatal Intra-Amniotic Endotoxin Induces Fetal Gut and Lung Immune Responses and Postnatal Systemic Inflammation in Preterm Pigs. *Am. J. Pathol.* **188**, 2629–2643. https://doi.org/10.1016/j.ajpath.2018.07.020 (2018).
68. Fricke, E. M. et al. Lipopolysaccharide-induced maternal inflammation induces direct placental injury without alteration in placental blood flow and induces a secondary fetal intestinal injury that persists into adulthood. *Am. J. Reprod. Immunol.* **79**, e12816. https://doi.org/10.1111/aji.12816 (2018).
69. Lin, Z. et al. Genetic Association of Pulmonary Surfactant Protein Genes, SFTPA1, SFTPA2, SFTPB, SFTPC, and SFTPD With Cystic Fibrosis. *Front. Immunol.* **9**, 2256. https://doi.org/10.3389/fimmu.2018.02256 (2018).
70. Dowd, J. B., Zajacova, A. & Aiello, A. Early origins of health disparities: burden of infection, health, and socioeconomic status in U.S. children. *Soc. Sci. Med.* **68**, 699–707. https://doi.org/10.1016/j.socscimed.2008.12.010 (2009).
71. Griffiths, P. S., Walton, C., Samsell, L., Perez, M. K. & Piedimonte, G. Maternal high-fat hypercaloric diet during pregnancy results in persistent metabolic and respiratory abnormalities in offspring. *Pediatr. Res.* **79**, 278–286. https://doi.org/10.1038/pr.2015.226 (2016).
72. Sureshchandra, S. et al. Maternal obesity blunts antimicrobial responses in fetal monocytes. *Elife* **12** https://doi.org/10.7554/eLife.81320 (2023).
73. López, D. A. et al. Prenatal inflammation perturbs murine fetal hematopoietic development and causes persistent changes to postnatal immunity. *Cell. Rep.* **41**, 111677. https://doi.org/10.1016/j.celrep.2022.111677 (2022).
74. Nash, M. J. et al. Maternal diet alters long-term innate immune cell memory in fetal and juvenile hematopoietic stem and progenitor cells in nonhuman primate offspring. *Cell. Rep.* **42**, 112393. https://doi.org/10.1016/j.celrep.2023.112393 (2023).
75. Cifuentes-Zúñiga, F. et al. IL-10 expression in macrophages from neonates born from obese mothers is suppressed by IL-4 and LPS/INFγ. *J. Cell. Physiol.* **232**, 3693–3701. https://doi.org/10.1002/jcp.25845 (2017).
76. Neehus, A. L. et al. Human inherited CCR2 deficiency underlies progressive polycystic lung disease. *Cell* **187**, 390–408e323. https://doi.org/10.1016/j.cell.2023.11.036 (2024).
77. He, Y. et al. Gut-lung axis: The microbial contributions and clinical implications. *Crit. Rev. Microbiol.* **43**, 81–95. https://doi.org/10.1080/1040841x.2016.1176988 (2017).
78. Groschwitz, K. R. & Hogan, S. P. Intestinal barrier function: molecular regulation and disease pathogenesis. *J Allergy Clin Immunol* 124, 3–20; quiz 21–22 (2009). https://doi.org/10.1016/j.jaci.2009.05.038
79. Kumar, M. et al. Increased intestinal permeability exacerbates sepsis through reduced hepatic SCD-1 activity and dysregulated iron recycling. *Nat. Commun.* **11**, 483 (2020).

80. Ranjbar, R., Vahdati, S. N., Tavakoli, S., Khodaie, R. & Behboudi, H. Immunomodulatory roles of microbiota-derived short-chain fatty acids in bacterial infections. *Biomed. Pharmacother*. **141**, 111817. https://doi.org/10.1016/j.biopha.2021.111817 (2021).
81. Verma, A. et al. Short-Chain Fatty Acid (SCFA) as a Connecting Link between Microbiota and Gut-Lung Axis-A Potential Therapeutic Intervention to Improve Lung Health. *ACS Omega*. **9**, 14648–14671. https://doi.org/10.1021/acsomega.3c05846 (2024).
82. Yan, Q., Jia, S., Li, D. & Yang, J. The role and mechanism of action of microbiota-derived short-chain fatty acids in neutrophils: From the activation to becoming potential biomarkers. *Biomed. Pharmacother*. **169**, 115821. https://doi.org/10.1016/j.biopha.2023.115821 (2023).
83. Galley, J. D., Bailey, M., Kamp Dush, C., Schoppe-Sullivan, S. & Christian, L. M. Maternal obesity is associated with alterations in the gut microbiome in toddlers. *PLoS One*. **9**, e113026. https://doi.org/10.1371/journal.pone.0113026 (2014).
84. Gilley, S. P. et al. Associations between maternal obesity and offspring gut microbiome in the first year of life. *Pediatr. Obes.* **17**, e12921. https://doi.org/10.1111/ijpo.12921 (2022).
85. Guo, Y. et al. Diet induced maternal obesity affects offspring gut microbiota and persists into young adulthood. *Food Funct.* **9**, 4317–4327. https://doi.org/10.1039/c8fo00444g (2018).
86. Soderborg, T. K. et al. The gut microbiota in infants of obese mothers increases inflammation and susceptibility to NAFLD. *Nat. Commun.* **9**, 4462 (2018).
87. Tonetti, F. R., Eguileor, A. & Llorente, C. Goblet cells: guardians of gut immunity and their role in gastrointestinal diseases. *eGastroenterology* **2** https://doi.org/10.1136/egastro-2024-100098 (2024).
88. Nash, M. J. et al. Maternal diet alters long-term innate immune cell memory in fetal and juvenile hematopoietic stem and progenitor cells in nonhuman primate offspring. *Cell reports* **42** (2023).
89. Bahadoran, A., Bezavada, L. & Smallwood, H. S. Fueling influenza and the immune response: Implications for metabolic reprogramming during influenza infection and immunometabolism. *Immunol. Rev.* **295**, 140–166. https://doi.org/10.1111/imr.12851 (2020).

Figures

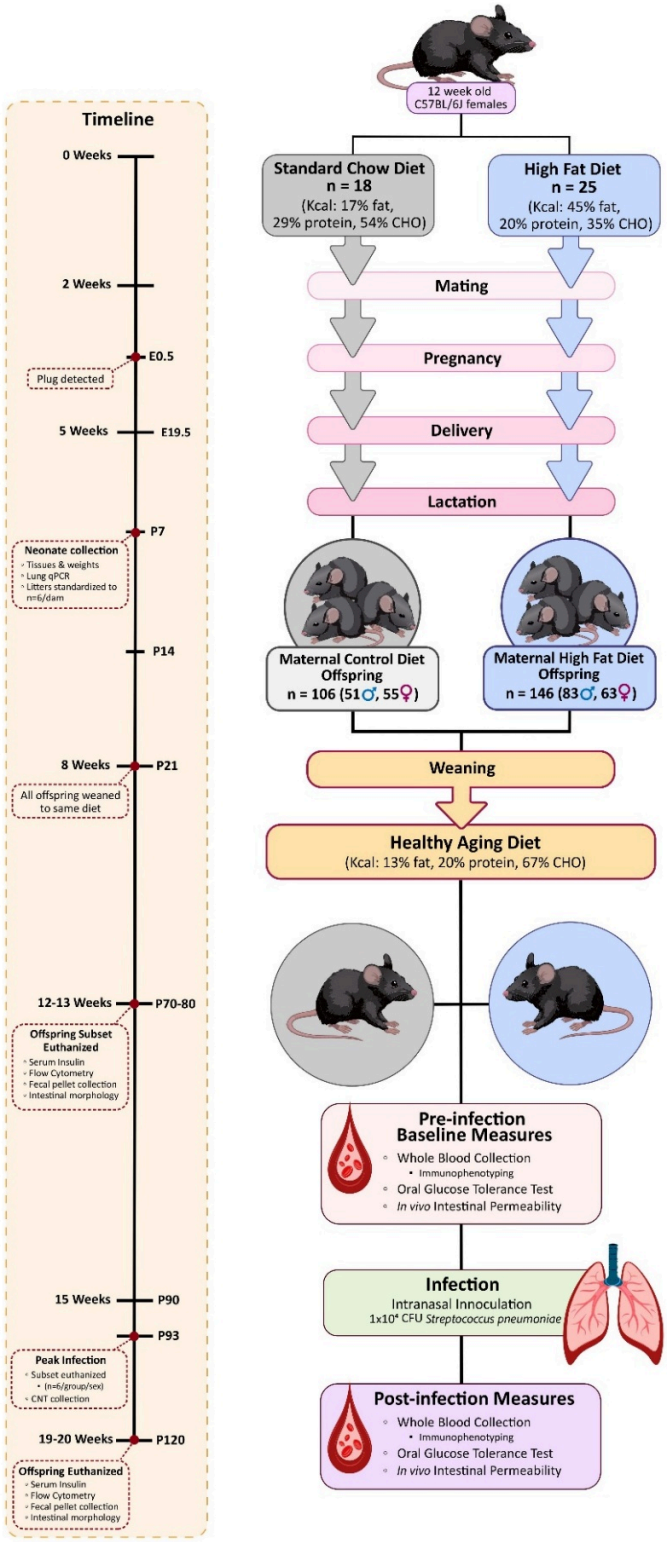
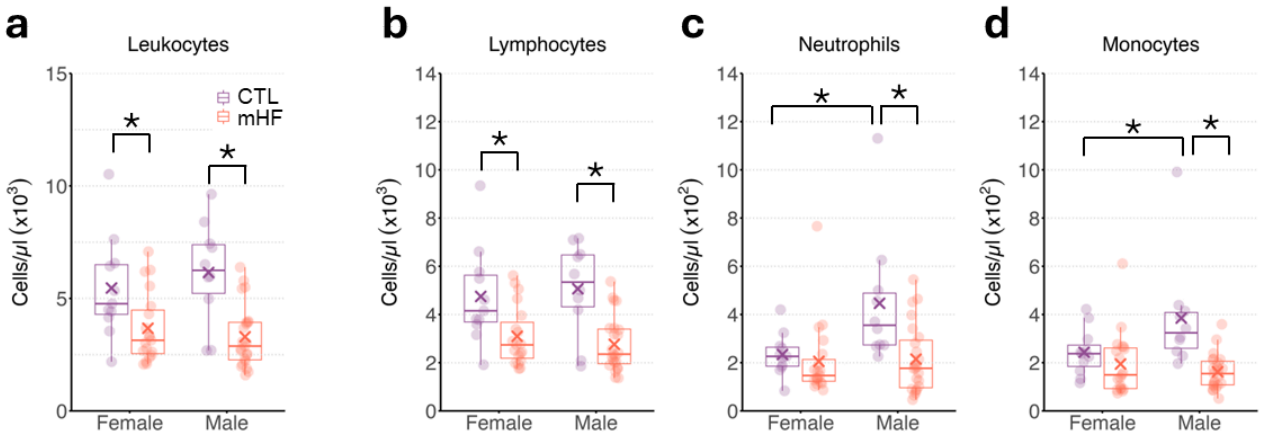


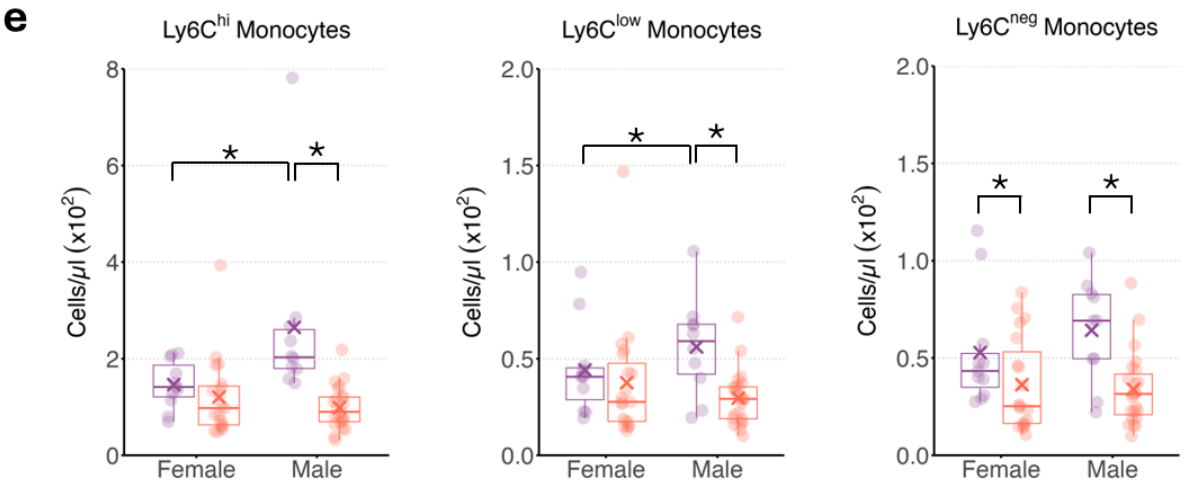
Figure 1

experimental design



Factor	p-value
diet	<0.001
sex	0.720
diet x sex	0.221

Factor	p-value		
	Lymphocytes	***Neutrophils***	***Monocytes***
diet	<0.001	0.010	0.001
sex	0.964	0.012	0.112
diet x sex	0.374	0.021	0.014



Factor	p-value		
	Ly6C^{hi}	***Ly6C^{low}***	***Ly6C^{neg}***
diet	<0.001	0.024	0.005
sex	0.055	0.759	0.460
diet x sex	0.007	0.114	0.317

Figure 2

Absolute counts of circulating immune cells pre-infection in offspring. Flow cytometry analysis of total leukocyte **a)**, lymphocyte, **b)**, neutrophil, **(c)**, and monocyte, **d)** absolute counts (cells/µL) in female (F) and male (M) offspring from dams fed either a control (CTL) or a maternal high-fat (mHF) diet, and**e)** Subsets of monocytes, including Ly6C^{hi}, Ly6C^{low}, and Ly6C^{neg}, were quantified. Boxplots represent the median and interquartile range, with individual data points overlaid. Asterisks indicate statistically

significant differences ($p < 0.05$). The tables summarize p-values from statistical analyses assessing the effects of diet, sex, and their interaction (diet × sex), with statistically significant values ($p < 0.05$) highlighted.

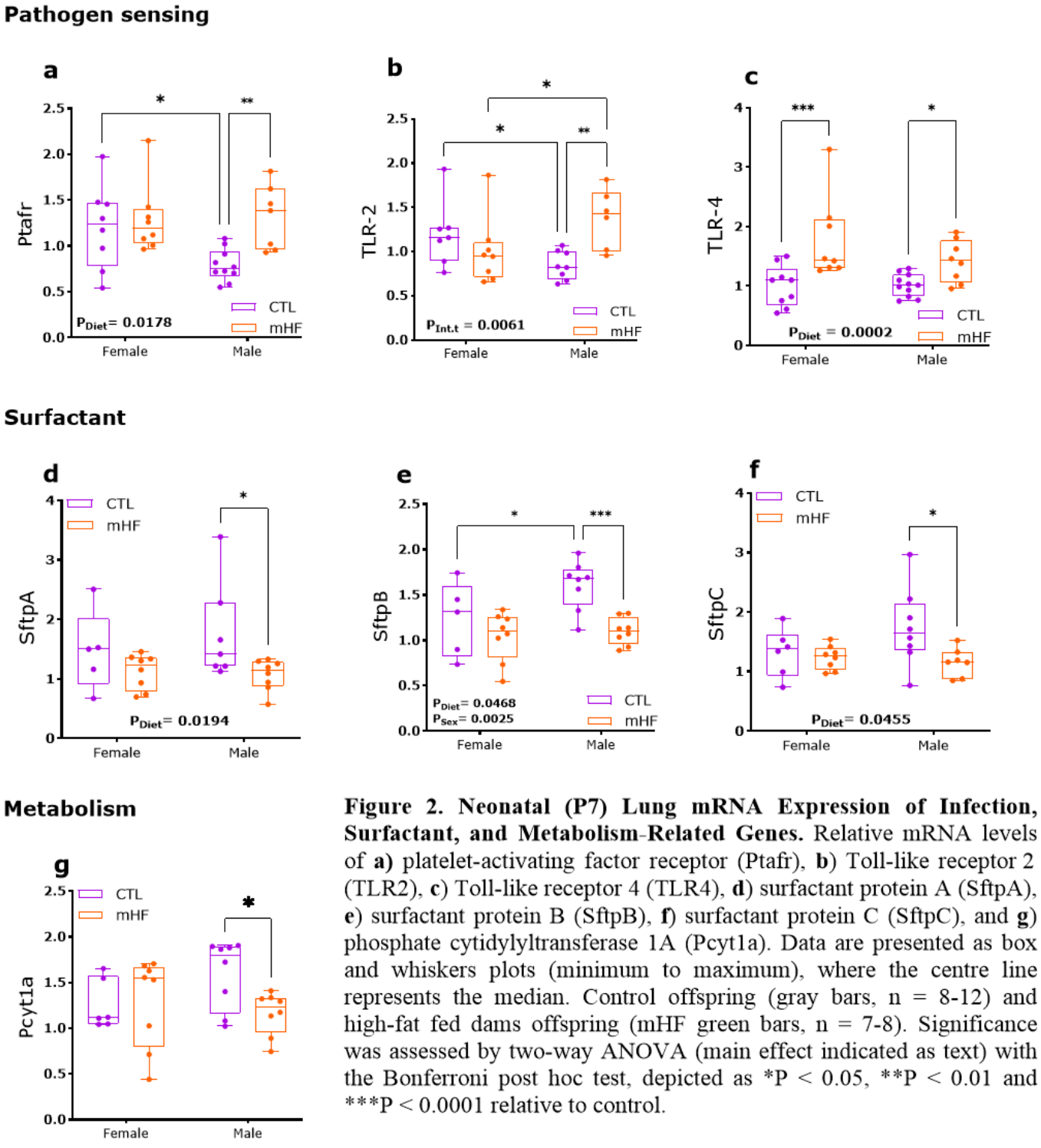
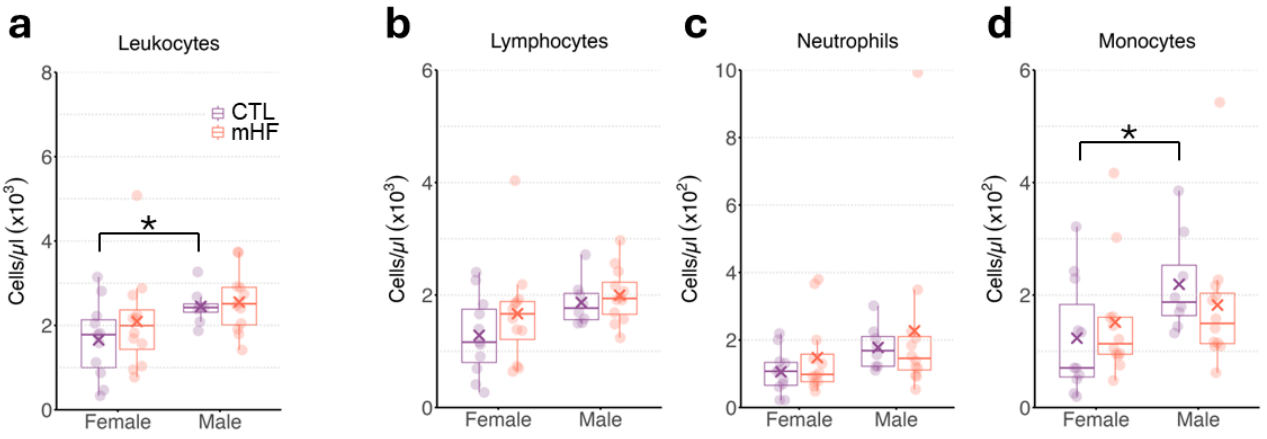


Figure 2. Neonatal (P7) Lung mRNA Expression of Infection, Surfactant, and Metabolism-Related Genes. Relative mRNA levels of **a)** platelet-activating factor receptor (Ptafr), **b**) Toll-like receptor 2 (TLR2), **c**) Toll-like receptor 4 (TLR4), **d**) surfactant protein A (SftpA), **e**) surfactant protein B (SftpB), **f**) surfactant protein C (SftpC), and **g**) phosphate cytidylyltransferase 1A (Pcyt1a). Data are presented as box and whiskers plots (minimum to maximum), where the centre line represents the median. Control offspring (gray bars, n = 8-12) and high-fat fed dams offspring (mHF green bars, n = 7-8). Significance was assessed by two-way ANOVA (main effect indicated as text) with the Bonferroni post hoc test, depicted as *P < 0.05, **P < 0.01 and ***P < 0.0001 relative to control.

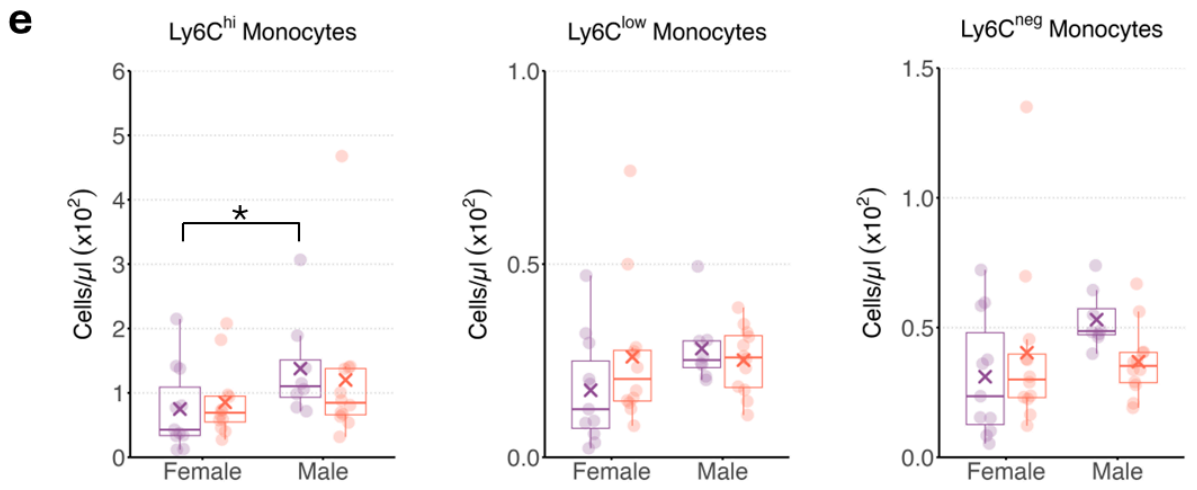
Figure 3

See image above for figure legend



Factor	p-value
diet	0.377
sex	0.010
diet x sex	0.473

Factor	p-value		
	Lymphocytes	***Neutrophils***	***Monocytes***
diet	0.475	0.255	0.772
sex	0.043	0.024	0.016
diet x sex	0.956	0.533	0.179

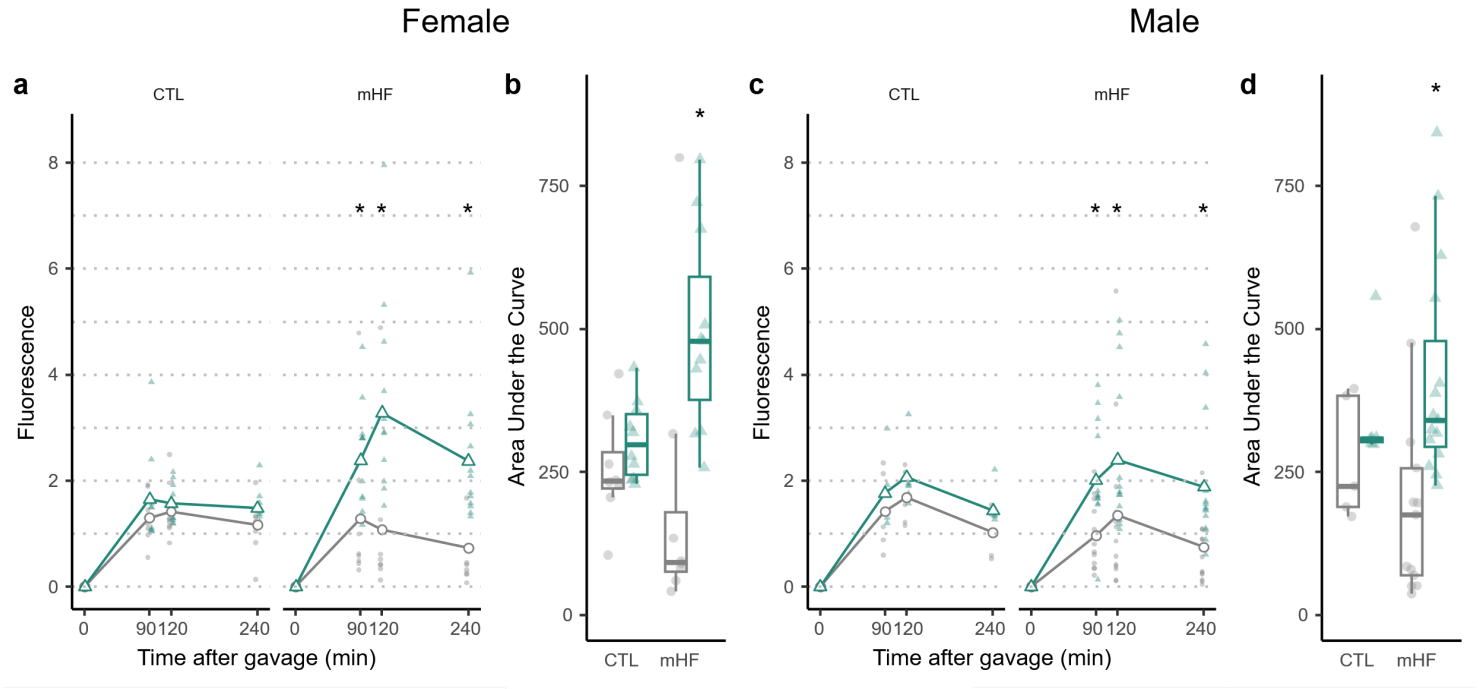


Factor	p-value		
	Ly6C^{hi}	***Ly6C^{low}***	***Ly6C^{neg}***
diet	0.799	0.616	0.622
sex	0.018	0.179	0.198
diet x sex	0.453	0.101	0.084

Figure 4

Absolute counts of circulating immune cells 30 days post-infection in offspring. Flow cytometry analysis of leukocyte **a),** lymphocyte**, b)** neutrophil, **c),** monocyte, **d)** absolute counts (cells/µL) in female (F) and male (M) offspring from dams fed either a control (CTL) or a maternal high-fat (mHF) diet, and **e)** Subsets of monocytes, including Ly6C^{hi}, Ly6C^{low}, and Ly6C^{neg}, were quantified. Boxplots represent the median and interquartile range, with individual data points overlaid. Different letters indicate statistically

significant differences ($p < 0.05$). The tables summarize p-values from statistical analyses assessing the effects of diet, sex, and their interaction (diet × sex), with statistically significant values ($p < 0.05$) highlighted.

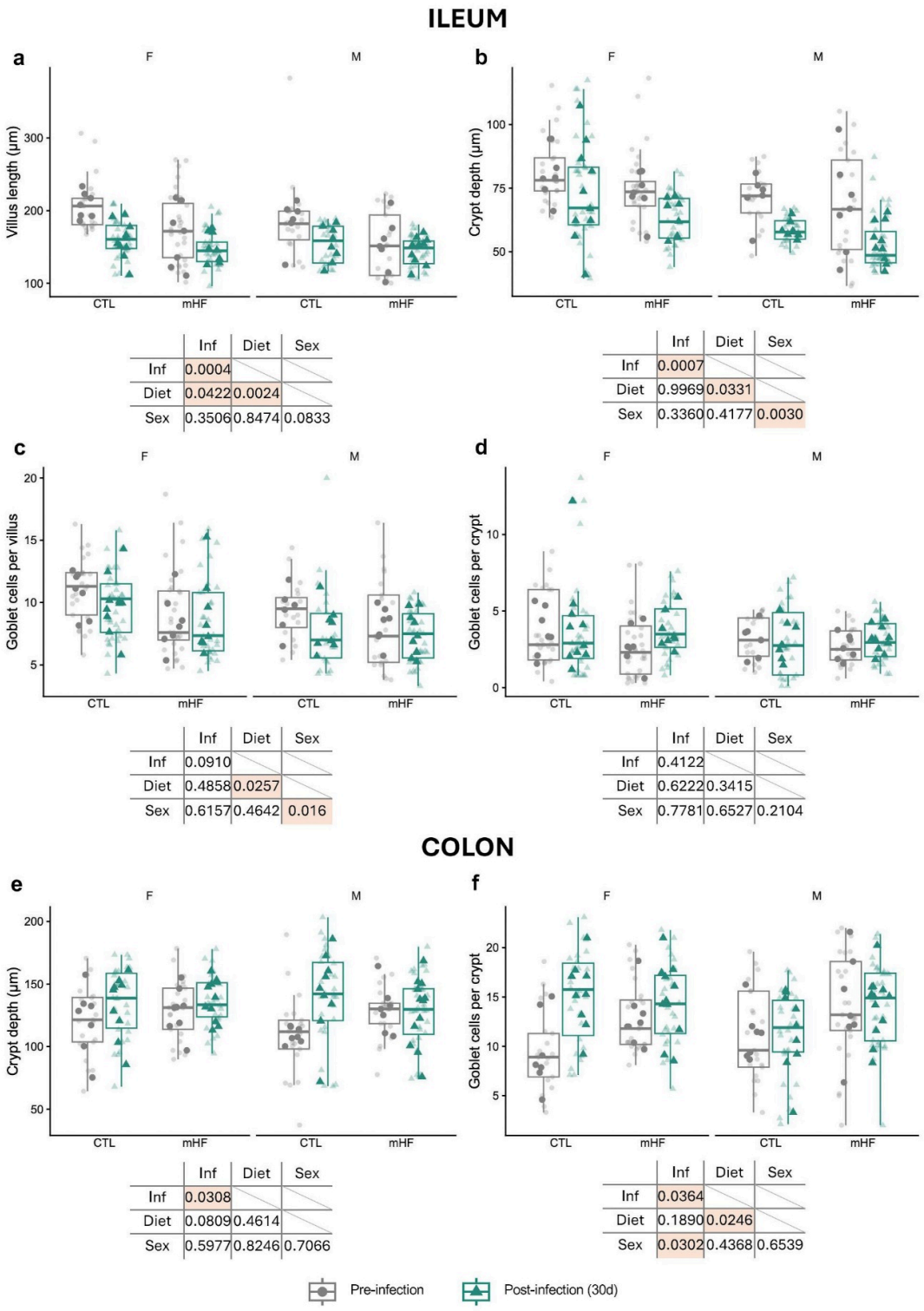


FITC	Inf	Diet	Sex	Time
Inf	2.015e-08			
Diet	0.0003	0.4324925		
Sex	0.3427	0.1127	0.8760	
Time	0.0028	0.6746	6.898e-10	<2.2e-16

AUC	Inf	Diet	Sex
Inf	7e-05		
Diet	0.0103	0.3971	
Sex	0.5545	0.1228	0.4035

Figure 5

Effects of maternal high-fat diet and pneumonia infection on intestinal permeability in offspring. Fluorescence intensity following FITC-dextran gavage in **a)** female and **c)** male offspring from dams fed either a control (CTL) or (mHF) diet, measured pre-infection (gray circles) and 30 days post-infection (green triangles) represented as individual datapoints (closed circles and triangles) and means (open circles and triangles). **(b, d)** Area under the curve (AUC) analysis of fluorescence intensity in **b)** female and **d)** male offspring are represented as box plots displaying median, interquartile range, and individual data points. The tables summarize main and interaction effect p-values from statistical analyses evaluating the effects of infection (Inf), diet, sex, and time on intestinal permeability, with $p < 0.05$ highlighted. Asterisks (*) denote *post-hoc* significant difference as compared to pre-infection ($p < 0.05$) within diet, sex, and time groups, where applicable.



	Inf	Diet	Sex
Inf	0.0004		
Diet	0.0422	0.0024	
Sex	0.3506	0.8474	0.0833

	Inf	Diet	Sex
Inf	0.0007		
Diet	0.9969	0.0331	
Sex	0.3360	0.4177	0.0030

	Inf	Diet	Sex
Inf	0.0910		
Diet	0.4858	0.0257	
Sex	0.6157	0.4642	0.016

	Inf	Diet	Sex
Inf	0.4122		
Diet	0.6222	0.3415	
Sex	0.7781	0.6527	0.2104

	Inf	Diet	Sex
Inf	0.0308		
Diet	0.0809	0.4614	
Sex	0.5977	0.8246	0.7066

	Inf	Diet	Sex
Inf	0.0364		
Diet	0.1890	0.0246	
Sex	0.0302	0.4368	0.6539

Figure 6

Effects of maternal high-fat diet and pneumonia infection on intestinal morphology and goblet cell abundance. **a)** Ileum villus length, **b)** ileum crypt depth, **c)**villus-associated goblet cell abundance, **d)** crypt-associated goblet cell abundance, (e colon crypt depth, and f) colon goblet cell abundance were quantified from histological sections stained with Alcian blue collected pre- (P90) and post-infection (P120) from female (F) and male (M) offspring of control (CTL) or maternal high-fat diet (mHF) dams.

Data are shown as box plots (median = center line; box = first and third quartiles; solid points = individual mice, transparent points = histological sections). Statistical analysis by linear mixed-effects models and type III ANOVA, with main and interaction effect p-values for infection (Inf), maternal diet, and sex with p<0.05 highlighted summarized in tables. Asterisks (*) denote *post-hoc* significant difference as compared to pre-infection (p < 0.05) within diet and sex.

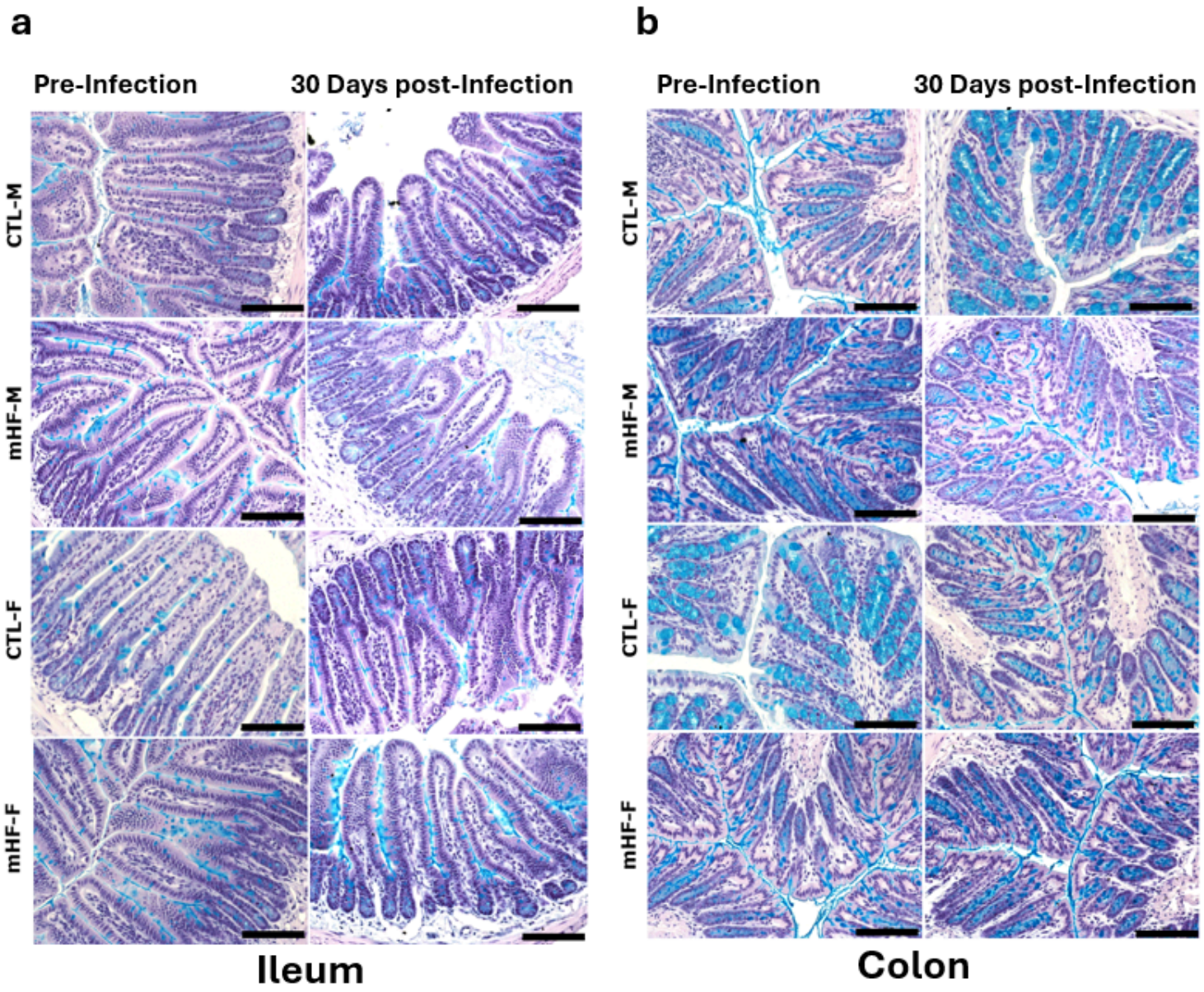


Figure 7

Representative images of ileum and colon histology pre- and post-infection in male and female offspring from control (CTL) and maternal high-fat diet (mHF) groups. a) Ileum and **b**) colon sections stained with Alcian blue to measure villi and crypt depth length and visualize goblet cells and mucin production. Images are shown for both male (M) and female (F) offspring from dams fed either a control (CTL) or (mHF) diet, before infection (P90) and 30 days post-pneumonia infection (P120). Scale bars: 100 μm.

Supplementary Files

This is a list of supplementary files associated with this preprint. Click to download.

- SuplementaryMaterialMaternaldietinducedexcessadiposityprograms.docx